Solution and Solid-state Nuclear Magnetic Resonance Studies on Interstitial Atoms within Transition-metal Carbonyl Clusters

Brian T. Heaton,[a] Jonathan A. Iggo,[a] Giuliano Longoni[b] and Suzanne Mulley[a]
[a] *Department of Chemistry, University of Liverpool, Liverpool L69 3BX, UK*
[b] *Dipartimento di Chimica Fisica ed Inorganica, Università di Bologna, 41034 Bologna, Italy*

The bonding of the interstitial atoms (C and N) within the metal skeleton in a series of transition-metal carbonyl clusters has been investigated by NMR studies of the shielding anisotropy and asymmetry in solution and in the solid state. Observed shielding anisotropies suggest that the hybridisation of the interstitial atom is dependent on the metal geometry and tends towards sp in an octahedral, sp^2 in a trigonal-prismatic and sp^3 in a square-antiprismatic metal skeleton.

NMR spectroscopy has long been used as an analytical tool for determining molecular composition but now with the advance of more sophisticated instrumentation, detailed information about the interactions of nuclei such as bond strength, type and length may be obtained.[1,2] For example, in clusters, the hybridisation of interstitial atoms may be determined from the shielding anisotropy (SA). A large SA is found for nuclei that have sp or sp^2 hybridisation, whereas sp^3 hybridisation gives rise to a very small anisotropy due to the symmetrical distribution of the orbitals around the nucleus. Thus, Gleeson and Vaughan[3] have shown that the carbon atoms in carbonyl ligands on various transition-metal clusters have large anisotropies consistent with sp hybridisation.

The SA can be determined either from an analysis of the solution spin-lattice relaxation or from the solid-state NMR line-shape. We now report the results of our study of the hybridisation of the interstitial atoms contained within transition-metal cluster polyhedra determined from measurements of the SA both in solution and in the solid state.

Results and Discussion

A wide variety of metal geometries are now known for transition-metal carbonyl clusters containing interstitial atoms. We have selected a series of compounds, $[Co_6E(CO)_{15/13}]^{n-}$, $[Rh_6E(CO)_{15/13}]^{n-}$ (E = C, N, n = 2, 1 respectively), $[Ni_8C(CO)_{16}]^{2-}$, $[Ni_9C(CO)_{17}]^{2-}$ and $[Ni_{10}C(CO)_{18}]^{2-}$, which adopt octahedral, trigonal-prismatic or square-antiprismatic (with one- and two-caps) metal geometries, in order to assess the effect of geometry and the influence of the metal polyhedron encapsulating the interstitial atom on the bonding of the interstitial atom. The effect of the chemical nature of the interstitial in the rhodium and cobalt analogues was analysed by the substitution of nitride for carbide in the interstitial position.

Solution-state Measurements.—In order to be able to correlate the amount of SA of a particular atom with the hybridisation it possesses one must first determine a numerical value for the SA. Equation (1) shows the relationship between

$$\frac{1}{T_1} = \frac{2}{15}\gamma_A^2 B_0^2 \Delta\sigma^2 \tau_c \qquad (1)$$

T_1, SA and the applied magnetic field for a tumbling molecule in solution, where γ_A is the gyromagnetic ratio of nucleus A, $\Delta\sigma$ is the shielding anisotropy, B_0 the applied magnetic field and τ_c the correlation time.

Table 1 Relaxation times for the interstitial atoms in various transition-metal clusters in acetone solution at room temperature

	T_1/s	
Compound	B = 4.7 T	9.4 T
$[N(PPh_3)_2]_2[Rh_6{}^{13}C(CO)_{15}]$	4.2	1.2
$[N(PPh_3)_2]_2[Rh_6{}^{13}C(CO)_{13}]$	10.9	1.6
$[N(PPh_3)_2][Rh_6{}^{15}N(CO)_{15}]$	110.0	24.7
$[N(PPh_3)_2][Rh_6{}^{15}N(CO)_{13}]$	32.4[a]	
$[NEt_3(CH_2Ph)]_2[Co_6{}^{13}C(CO)_{15}]$	3.2	2.0
$[NEt_3(CH_2Ph)]_2[Co_6{}^{13}C(CO)_{13}]$	5.0	4.1
$[N(PPh_3)_2][Co_6{}^{15}N(CO)_{15}]$	14.2	12.8
$[N(PPh_3)_2][Co_6{}^{14}N(CO)_{15}]$	0.01	—
$[N(PPh_3)_2][Co_6{}^{14}N(CO)_{13}]$	0.02	—
$[NMe_3(CH_2Ph)]_2[Ni_{10}{}^{13}C(CO)_{18}]$	325.0	274.1[b]
$[NMe_3(CH_2Ph)]_2[Ni_9{}^{13}C(CO)_{17}]$	—	183.0

[a] Some sample decomposition was noted. [b] Measured at 6.3 T; the contribution to the relaxation by scalar coupling, spin rotation and unpaired electron pathways can be shown to be negligible.

As can be seen, the T_1 of a nucleus relaxing principally *via* the shielding anisotropy mechanism will show a strong dependence on the applied magnetic field. Therefore T_1 relaxation data were obtained at 4.7 and 9.4 T, using the inversion recovery method for the carbides with shorter T_1 values and the saturation recovery method for the carbides and the nitrides having longer relaxation times. Table 1 gives the T_1 data obtained in solution for all the compounds studied. In all cases, the relaxation time for ^{15}N was considerably longer than that for ^{13}C in analogous compounds, as expected given the difference in gyromagnetic ratios of the two nuclei ($\gamma_{^{15}N} = -2.72 \times 10^7$, $\gamma_{^{13}C} = 6.7 \times 10^7$ rad T^{-1} s^{-1}).

The overall relaxation is the sum of all of the various contributive mechanisms in operation, equation (2), where

$$\frac{1}{T_{1obs}} = \frac{1}{T_{1DD}} + \frac{1}{T_{1SA}} + \frac{1}{T_{1SC}} + \frac{1}{T_{1SR}} + \frac{1}{T_{1UE}} + \frac{1}{T_{1Q}} \qquad (2)$$

T_{1DD} = dipolar, T_{1SA} = shielding anisotropy, T_{1SC} = scalar coupling, T_{1SR} = spin rotation, T_{1UE} = unpaired electron and T_{1Q} = spin–quadrupole, relaxation.

Considering the particular systems under study, a qualitative approximation of the relative contributions to the overall relaxation may be made. Relaxation *via* the scalar-coupling mechanism may be ruled out because there is no chemical exchange occurring in the systems studied, therefore the coupling between the interstitial atom and the neighbouring metal atoms is not time dependent. A scalar interaction of the second kind can occur if the nuclear spin coupling to the interstitial nucleus is a fast relaxing quadrupole and the resonance frequencies of the quadrupolar nucleus and the observed nucleus are similar (as in the case of ^{13}C–^{79}Br; 25.145 and 25.13 MHz respectively at 2.35 T).[2] If not, the denominator of the relaxation expression becomes very large which then gives unacceptable values for either T_1 or τ_{SC}. Comparison of the T_1 values of the compounds of Rh and Co reiterates this point; much shorter relaxation times would have been expected (*i.e.* at least an order of magnitude shorter) for the cobalt compounds had the quadrupolar moment of the Co been playing any part in the relaxation, whereas in actual fact the T_1 values are found to be very similar (Table 1).

Great care was taken during sample preparation to eliminate paramagnetic impurities so there should be no contribution to the overall relaxation by unpaired electrons. The absence of paramagnetic impurities in the samples is confirmed by the observation that the slowly relaxing rhodium clusters closely follow the field dependency characteristic of shielding anisotropy relaxation (see below).

The spin–rotation interaction depends upon the moment of inertia of the molecule and the spin interaction constant and is most important for spin-$\frac{1}{2}$ nuclei in small molecules, particularly in the gas phase.[4] Given the size of the molecules (35–47 atoms) it is unlikely that the spin–rotation contribution to relaxation will be significant in the present case. Furthermore, the relaxing interstitial nuclei are in fixed positions relative to the metal skeleton. The absence of spin–rotation relaxation is confirmed by the following observation. For spherical molecules, τ_{SC} (the time between collisions causing spin–rotation relaxation) is inversely proportional to τ_c (the conventional correlation time).[5] Since the correlation time τ_c is not expected to change significantly between the various hexanuclear clusters studied, the spin–rotation correlation time and hence $(\tau_{SC})^{-1}$ will be proportional to the moment of inertia, which in turn depends upon the mass of the molecule. A comparison of analogous rhodium and cobalt clusters shows that were spin rotation a significant relaxation pathway, a hundred-fold difference between the two series of T_1 values would be observed. This is not the case therefore relaxation *via* spin rotation may be ignored.

Quadrupolar relaxation may be eliminated as a possible pathway as neither ^{15}N nor ^{13}C are quadrupolar. The effect of a quadrupolar relaxing nucleus can be seen in the examples $[N(PPh_3)_2][Co_6{}^{14}N(CO)_{15}]$ and $[N(PPh_3)_2][Co_6{}^{14}N(CO)_{13}]$ which have T_1 values of 0.01 and 0.02 s respectively compared to 14.2 s for $[N(PPh_3)_2][Co_6{}^{15}N(CO)_{15}]$. The natural abundance of the quadrupolar ^{61}Ni isotope (1.19%) is too low for quadrupolar relaxation to have any observable effect on the relaxation of the carbide in the nickel clusters.

The major relaxation pathways for the interstitial atoms must then be SA and dipole–dipole so that equation (2) simplifies to equation (3).

$$\frac{1}{T_{1obs}} = \frac{1}{T_{1DD}} + \frac{1}{T_{1SA}} \qquad (3)$$

The relative contributions of the two relaxation pathways can be evaluated since T_{1SA} is field dependent [equation (1)] whereas T_{1DD} is field independent in the extreme narrowing limit [equation (4)]; therefore a plot of $(T_{1obs})^{-1}$ against $B_0{}^2$ will give a straight-line graph, the intercept of which gives a value for $(T_{1DD})^{-1}$, hence the relative contributions of both mechanisms may be estimated.

$$\frac{1}{T_1} = \left(\frac{\mu_0}{4\pi}\right)^2 \gamma_A{}^2\gamma_X{}^2 h\tau_c/r^6 \qquad (4)$$

Cobalt and Rhodium Complexes.—Using the method described above an estimation of the relative contributions to the relaxation of each cluster compound was made. For the cobalt clusters at low field, the dipole–dipole interaction accounts for 80–90% of the relaxation of the interstitial atom, decreasing to 50–70% at high field where the shielding anisotropy mechanism is relatively more important. Comparison of the data for the cobalt nitride and carbide clusters shows an increased importance of the dipole–dipole interaction for the nitride complex ions in which it is responsible for 85–90% of the relaxation.

Conversely, the relaxation times of the rhodium clusters were found to be inversely proportional to the square of the field at which they were measured indicating that the predominant relaxation mechanism is shielding anisotropy which accounts for 85–90% of the relaxation. The T_1 values for the nitride analogues are much longer than the carbide ones but still demonstrate a strong field dependency indicating that shielding anisotropy is again the most important relaxation mechanism, accounting for *ca.* 90% of the total. The longer relaxation times observed in all cases when ^{15}N is substituted for ^{13}C must therefore be connected with the nature of the nitride itself and is in part linked to the fact that ^{15}N has a negative nuclear Overhauser effect (NOE). However, the smaller radius of the interstitial nitride compared with the carbide and the shorter M–N bonds[6] also contributes towards the increased importance of dipole–dipole relaxation in the nitride compounds with respect to their carbide analogues.

The difference in the dominant relaxation pathway between cobalt and rhodium clusters is due principally to the lower gyromagnetic ratio of ^{103}Rh since dipole–dipole relaxation depends upon the correlation time of the tumbling molecule, the internuclear distance and the product of the squares of the gyromagnetic ratios involved in the relaxation, equation (5).[7]

$$1/T_{1DD} \propto \gamma_M{}^2\gamma_C{}^2/r_{M\text{-}C}{}^6 \qquad (5)$$

Substitution of the appropriate values of γ and metal–carbide bond distance in equation (5) indicates that dipole–dipole relaxation will be *ca.* 95 times more efficient in the cobalt–carbide system than in the rhodium–carbide system. The T_1 values found for the cobalt clusters are shorter than those found for the rhodium clusters as dipole–dipole relaxation is a more efficient mechanism than shielding anisotropy.

Nickel Complexes.—The nickel carbide clusters do not exactly follow the field dependency expected for SA relaxation, an analysis of the type carried out above indicating that only *ca.* 70% of the relaxation is due to SA and the remaining 30% of the overall relaxation is achieved by some other mechanism. Unlike cobalt and rhodium the most abundant nickel isotopes have zero nuclear spin; ^{61}Ni, has a nuclear spin of $\frac{3}{2}$ but a natural abundance of only 1.19%, however, since there are 8–10 Ni atoms per molecule in the samples, dipole–dipole relaxation can occur in *ca.* 10% of molecules that contain at least one ^{61}Ni. This contribution, however, is very small and will therefore result in a lengthening of the relaxation time overall. The very long T_1 values observed for the nickel clusters compared to the rhodium cluster systems may also indicate a smaller SA for the interstitial carbide in the nickel clusters since the principal relaxation path in both the nickel and rhodium series is SA. This in turn suggests a closer approach to sp^3 hybridisation for the nickel carbides. Certainly, the different metal geometry (square antiprismatic) around the carbon may promote a more symmetrical bonding pattern involving sp^3 hybridisation at the carbon.

Table 2 Shielding anisotropy and asymmetry parameters of the interstitial atom of various transition-metal clusters at 7.0 T

Compound	σ_{iso} [a]	ζ [b]	η [c]	Principal components of ζ		
				σ_{xx}	σ_{yy}	σ_{zz}
$[N(PPh_3)_2]_2[Rh_6{}^{13}C(CO)_{15}]$	−265	256	0.00	−393	−393	−9
$[N(PPh_3)_2]_2[Rh_6{}^{13}C(CO)_{13}]$	−472	−233	0.00	−349	−362	−705
$[N(PPh_3)_2][Rh_6{}^{15}N(CO)_{15}]$	264	208	0.00	−160	−160	472
$[NEt_3(CH_2Ph)]_2[Co_6{}^{13}C(CO)_{15}]$	−334	294	0.38	−537	−425	−40
$[N(PPh_3)_2][Co_6{}^{15}N(CO)_{15}]$	170	400 [d]	0.00	−30	−30	570
$[NEt_4]_2[Ni_8{}^{13}C(CO)_{16}]$	−380	73	0.74	−442	−389	−307
$[NMe_3(CH_2Ph)]_2[Ni_9{}^{13}C(CO)_{17}]$	−320	25	0.72	−341	−323	−295
$[NMe_3(CH_2Ph)]_2[Ni_{10}{}^{13}C(CO)_{18}]$	−278	−34	0.62	−251	−272	−312

[a] σ_{iso} = Isotropic chemical shift referenced to $SiMe_4$ for the carbide compounds and $MeNO_2$ for the nitride compounds. [b] ζ = Shielding anisotropy (ppm). [c] η = Asymmetry. [d] Rather approximate due to signal : noise ratio obscuring some of the side bands.

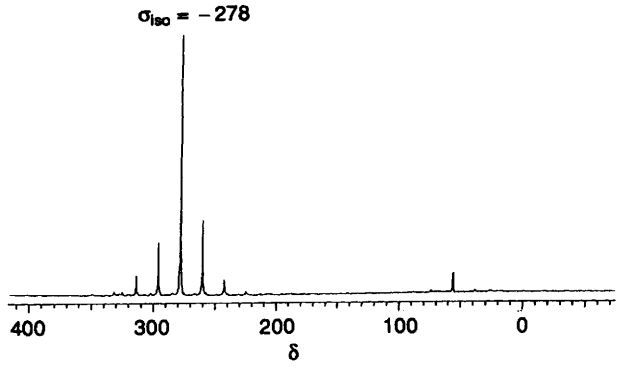

Fig. 1 Solid-state ^{13}C NMR spectrum of $[NMe_3(CH_2Ph)]_2[Ni_{10}C(CO)_{18}]$. Spin rate = 1350 Hz, ^{13}C resonance frequency = 75.431 MHz, relaxation delay = 2.0 s, no. of transients = 500, cross-polarisation contact time = 0.005 s; ζ = −34 ppm, η = 0.62

Since the principal relaxation pathway for the interstitial nuclei in the cobalt complexes is not SA, it is not possible to comment on the nature of the bonding of the interstitial atoms in these clusters from solution data alone. It is necessary to measure the SA from the solid-state NMR line-shape (obtained *via* an analysis of the spinning side bands).

Solid-state Data.—Table 2 gives the SA (ζ) and asymmetry (η) parameters for all the compounds studied, defined in equations (6) and (7) respectively where σ_{iso} is the isotropic

$$\zeta = \sigma_{zz} - \sigma_{iso} \quad (6)$$

$$\eta = (\sigma_{yy} - \sigma_{xx})/\zeta \quad (7)$$

chemical shift and σ_{xx}, σ_{yy} and σ_{zz} are the principal components of ζ. Asymmetry parameters provide an indication of the symmetry of the d orbitals around the relaxing nucleus. Small values for the SA are found for nuclei with spherical-type hybridisation *i.e.* sp^3, whereas asymmetries of zero and large SA values are found for nuclei in cylindrical environments and indicate sp or sp^2 hybridisation.

Nickel complexes. Molecular-orbital calculations carried out by others on all the nickel compounds in this study show that sp^3 hybridisation is favourable for the interstitial atom.[8] All the nickel compounds studied have relatively small SA values and asymmetries approaching 1, in keeping with these calculations, *e.g.* $[NMe_3(CH_2Ph)]_2[Ni_{10}{}^{13}C(CO)_{18}]$, Fig. 1, Table 2. However, the fact that the asymmetry values are not exactly unity (range 0.62–0.74) and that the SA values are non-zero indicates a distortion away from cubic towards cylindrical symmetry, with more electron density lying along the z axis than the x and y axes *i.e.* the hybridisation of the carbide is not pure sp^3. For the Ni_9 and Ni_{10} clusters, this is not altogether unexpected since the capping nickel atoms (which lie on the z axis) are known to be within bonding distance of the carbide. For the Ni_8 cluster a greater amount of electron density along the z axis may be explained by the fact that the orbitals on the nickel atoms do not point directly at the carbide, *i.e.* to the centre of the cluster, but rather to the centres of the two square faces of nickel atoms above and below the interstitial atom so that the spherical distribution of electron density around the carbide must elongate in the z direction in order to interact with the nickel orbitals. Also, it can be seen that η decreases as the number of capping atoms increases, *i.e.* 0.74, 0.72 and 0.62 for Ni_8, Ni_9 and Ni_{10} respectively which indicates that there is more electron density along the z axis in Ni_{10} than in Ni_8 as would be expected by the fact that there are two more nickel atoms along the z direction.

From these measurements it may be seen that the very long relaxation times observed for the nickel carbides in solution can be attributed to the small anisotropy resulting in inefficient SA relaxation compared to the rhodium and cobalt compounds and the absence of any other more efficient relaxation path (the dipole–dipole relaxation being extremely inefficient due to the low concentration of ^{61}Ni).

Cobalt and rhodium complexes. The solid-state NMR data for the hexanuclear clusters, Table 2, show, in all cases, a large anisotropy indicating that the distribution of charge around the interstitial atom is not spherical. For most of the examples, the asymmetry was calculated to be zero indicating cylindrical symmetry, which leads to the conclusion that the carbide is either sp or sp^2 hybridised. The exception to this is $[Co_6{}^{13}C(CO)_{15}]^{2-}$ which gave an asymmetry value of 0.38. However, the spectrum obtained in the solid state (Fig. 2) for this compound has a rolling baseline and the outer spinning sidebands overlapped with the intense resonances (enhanced by efficient cross-polarisation) of the carbon atoms of the $NMe_3(CH_2Ph)$ cation. The detection of the most extreme spinning side bands of the carbide resonance was thus made difficult leading to errors in the estimation of ζ and η. Errors in η are likely to be more significant than those in ζ since σ_{xx} and σ_{yy} are generally found to be of similar magnitude but different from σ_{zz}, Table 2, equations (6) and (7) (see also Experimental section).

It is probable that the 'true' anisotropy of the carbide atom in $[Co_6{}^{13}C(CO)_{15}]^{2-}$ is close to zero, similar to the values found for other analogous compounds.

The octahedral cluster $[Rh_6{}^{13}C(CO)_{13}]^{2-}$ also exhibits a large anisotropy with zero asymmetry, again indicating either sp or sp^2 hybridisation. The negative sign of the anisotropy is a consequence of the definition of the principal components, σ_{xx}, σ_{yy} and σ_{zz} (usually assuming that $|\sigma_{zz} - \sigma_{iso}| > |\sigma_{xx} - \sigma_{iso}| > |\sigma_{yy} - \sigma_{iso}|$) and is manifested by the envelope of the spinning side bands being skewed in the opposite direction to

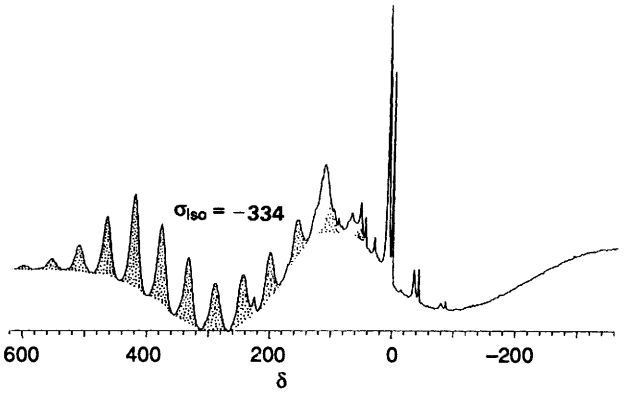

Fig. 2 Solid-state ^{13}C NMR spectrum of $[NMe_3(CH_2Ph)]_2[Co_6{}^{13}C(CO)_{15}]$. Spin rate = 3320 Hz, ^{13}C resonance frequency = 75.431 MHz, relaxation delay = 1.0 s, no. of transients = 38 200, cross-polarisation contact time = 0.005 s. Shaded areas denote peaks attributed to carbide resonance; ζ = 294 ppm, η = 0.38

that of $[Rh_6{}^{13}C(CO)_{15}]^{2-}$ (Fig. 3). In physical terms this reversal of anisotropy between the two compounds indicates that the hybridised orbitals of the interstitial atom in one cluster are orthogonal to those on the interstitial atom of the other cluster, considering their geometric relationship with the surrounding metal cage. In other words, the asymmetry parameters for $[Rh_6{}^{13}C(CO)_{15}]^{2-}$ and $[Rh_6{}^{13}C(CO)_{13}]^{2-}$ indicate that the interstitial atom has cylindrical symmetry *i.e.* sp or sp^2 hybridised in both cases, but one atom will be sp and the other sp^2 hybridised as indicated by the reversal in the anisotropy parameter.

From symmetry arguments, it is most likely that the interstitial atom in trigonal prisms is sp^2 with the three orbitals lying in the *xy* plane and pointing towards the edges of the prism rather than its square faces (see Fig. 4) permitting an equal interaction with all six metal atoms. When the same arguments are applied to the octahedral cluster, one finds that the three sp^2 lobes of an interstitial cannot interact equally with all six metal atoms. In the case of the clusters studied the octahedron is very distorted and may be considered as more of a trigonal antiprism, however, even so an sp^2 hybridised interstitial can only interact with three metal atoms at any time, and so an sp hybridisation is more favoured as it will promote a more symmetrical interaction, the two sp lobes pointing along the '*z*' axis of the metal cage with the remaining vacant p orbitals pointing to the four corners of the square in the equatorial plane of the metal cage thereby overlapping with the four equivalent metal atom orbitals (see Fig. 4).

In keeping with the above hybridisation assignment, previous vibrational studies have shown that there are two vibrations for the interstitial atom in the trigonal-prismatic species, associated with motion along, and perpendicular to, the three-fold symmetry axis of the clusters. The fact that two bands are observed at different energies indicates that bonding is not the same in all directions and supports the idea that the interstitial atom is either sp or sp^2 hybridised. The force constant in the equatorial plane was found to be slightly greater than that in the axial plane supporting the sp^2 hybridisation assigned above.[9] The cylindrical symmetry imposed by this hybridisation is consistent with the large anisotropies and asymmetry values observed.

A comparison of the fluxional behaviour in solution of the carbonyl ligands of the trigonal-prismatic and octahedral clusters also provides supporting evidence for the above assignment. In $[Rh_6{}^{13}C(CO)_{15}]^{2-}$ the carbonyls are constrained to the positions adopted in the solid state[10] in keeping with a homogeneous interaction of the interstitial orbitals with the six metal atoms. The solution NMR resonances for the carbonyls of $[Rh_6{}^{13}C(CO)_{13}]^{2-}$ on the other hand may only be explained by a fluxional arrangement of the seven carbonyl

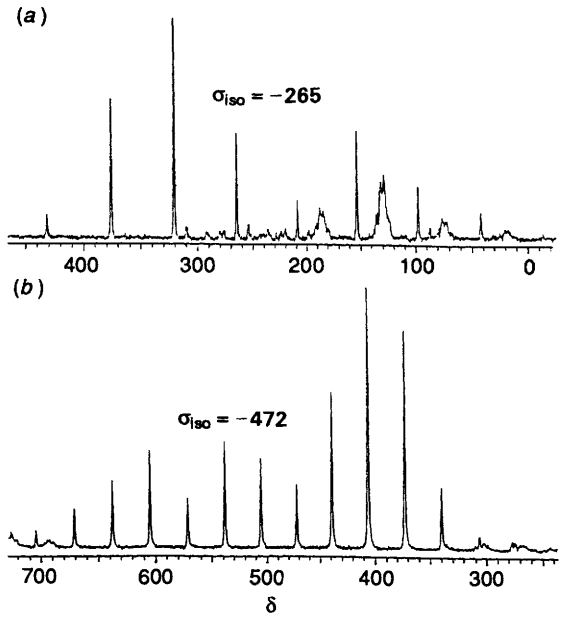

Fig. 3 Solid-state ^{13}C NMR spectra of (*a*) $[N(PPh_3)_2]_2[Rh_6{}^{13}C(CO)_{15}]$ (ζ = 256 ppm, η = 0.00) and (*b*) $[N(PPh_3)_2]_2[Rh_6{}^{13}C(CO)_{13}]$ (ζ = −233 ppm, η = 0.00). Spin rates 4200 and 2500 Hz respectively, ^{13}C resonance frequency = 75.431 MHz, relaxation delay = 2.0 s, no. of transients = 300 and 1000, cross-polarisation contact time = 0.005 s

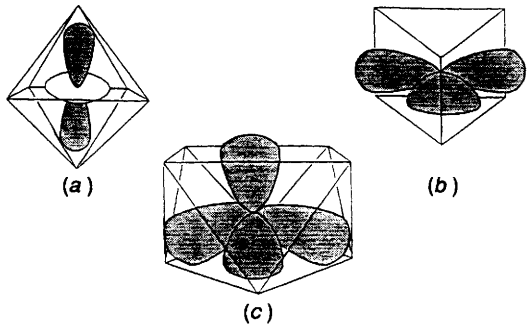

Fig. 4 Various metal polyhedra showing possible hybridisations of the interstitial atom; (*a*) octahedron, (*b*) trigonal prism, (*c*) square antiprism

ligands around the equatorial plane of the metal cage and X-ray measurements suggest a similar libration of these seven carbonyls in the solid state.[10] The remaining bridging and terminal carbonyls, those connected to the two apical metal atoms, are stationary[11] which would be consistent with the 'symmetrical' interaction of an sp hybridised interstitial.

In conclusion, this work has shown that the nature of the bonding of the interstitial atom can be determined fairly reliably from solid-state NMR data. Solution-state relaxation data may be useful when the relaxation is dominated by the SA provided data for a series of related compounds are available, but are also important in determining the relative significance of contributory factors to the overall relaxation.

It would seem that for the clusters studied so far, the hybridisation of the interstitial atom tends to sp in an octahedral environment, sp^2 in a trigonal-prismatic environment, and sp^3 in a square-antiprismatic environment and that it is this geometric environment which determines the hybridisation rather than *vice versa*. Generally, the introduction of an interstitial atom into a metal cage results in an enlargement of the cavity and a contemporary contraction of the interstitial itself. [This is demonstrated by the existence of an empty

trigonal-prismatic cavity in $Rh_6(CO)_{14}$.] The geometry of the metal framework adopted by the various compounds is determined by the number of electrons available for bonding and this then dictates both the cavity shape and size. Therefore, it seems logical to argue that the hybridisation adopted by an interstitial atom is that which fits best into the surrounding metal framework. Thus, octahedral clusters having an elongation or contraction along the z direction [Fig. 4(*a*)] allow accommodation of the sp orbitals in that direction, the trigonal prism is of the correct symmetry to accommodate the interstitial atom *via* three sp^2 orbitals whilst the larger square–antiprismatic nickel clusters can accommodate the interstitial atom *via* four sp^3 orbitals.

Larger interstitial atoms, such as P, Si, Ge and Sn, only fit into larger cavities and similar NMR studies could be used better to elucidate their mode of bonding.

Experimental

All NMR measurements in solution were carried out on Bruker WM 200 MHz or WM 400 MHz spectrometers except for the measurement on $[NMe_3(CH_2Ph)]_2[Ni_{10}{}^{13}C(CO)_{18}]$ which was made on a JEOL 300 MHz spectrometer.

The measurements in the solid state were all performed on a Varian VXR300 spectrometer using magic-angle spinning (MAS) and cross-polarisation routines. Typical contact times were 0.5 ms for most carbide compounds although 5 ms was sometimes used (in particular for those spectra shown in the figures); the spectra of nitride compounds were collected using contact times of 8 ms. Recycle delay times were generally in the range 1–5 s, although occasionally much longer delays were implemented. Calculation of ζ and η was carried out *via* an iterative fitting analysis of spinning sidebands*,[12] on spectra taken at two different sample spin speeds ranging from 620 to 4840 Hz for each sample. Variation in the values found for σ_{xx}, σ_{yy} and σ_{zz} at different spin rates was within 5% therefore the values calculated for ζ and η may be considered to be accurate to $\pm 10\%$, however cases where $\eta < 0.1$ are difficult to distinguish from those where $\eta = 0$, therefore for this work they have been treated as a single case. All samples were packed under nitrogen into specially designed inserts developed to handle air-sensitive compounds.[13]

Due to the air-sensitivity of all the compounds under study, syntheses were carried out using standard laboratory Schlenk apparatus under a nitrogen atmosphere. Solvents were all freshly distilled under N_2, over various drying agents; acetone over P_2O_5, acetonitrile, tetrahydrofuran, diisopropyl ether, toluene, pentane, hexane and Et_2O over Na and methanol and propan-2-ol over CaH_2. When needed, dimethylformamide was distilled under vacuum after being stirred for two days over anhydrous $CuSO_4$. All reactions were monitored by infrared spectroscopy, using cells (CaF_2 windows) which had been flushed with a stream of N_2 before introducing the reaction solution into the cell. As a last step in purification, all compounds were passed through a Celite filter to remove any paramagnetics and were thereafter only handled with glass apparatus.

Syntheses of the compounds studied were carried out following literature methods for the unenriched clusters, modifying the procedures so as to use the minimum amount of isotopically enriched materials, $[Ni_8{}^{13}C(CO)_{16}]^{2-}$, $[Ni_9{}^{13}C(CO)_{17}]^{2-}$, $[Ni_{10}{}^{13}C(CO)_{18}]^{2-}$,[14] $[Co_6{}^{13}C(CO)_{15}]^{2-}$,[15] $[Co_6{}^{13}C(CO)_{13}]^{2-}$,[16] $[Rh_6{}^{13}C(CO)_{15}]^{2-}$,[17] $[Rh_6{}^{13}C(CO)_{13}]^{2-}$,[18] $[Co_6{}^{15}N(CO)_{15}]^{-}$,[19] $[Co_6{}^{15}N(CO)_{13}]^{-}$[20] and $[Rh_6{}^{15}N(CO)_{15}]^{-}$.[21]

The labelled compounds $^{13}CCl_4$ (99% ^{13}C) and $NaNO_2$ (99% ^{15}N) were purchased from Strem and used directly and $[Ni_6(CO)_{12}]^{2-}$ was prepared as described by Longoni and co-workers.[22]

Acknowledgements

We thank Dr. G. Hawkes (Queen Mary and Westfield College), Dr. D. O. Smith (University of Kent) and Drs. D. C. Applerley and R. R Yeung of SERC solid-state NMR service (University of Durham) for NMR spectra and Professer A. Sironi (University of Milan) and Dr. D. Evans (University of Exeter) for helpful discussions. S. M. acknowledges the award of an SERC studentship and EC for the award of a studentship *via* the ERASMUS programme.

References

1 C. A. Fyfe, *Solid State NMR for Chemists*, C. F. C. Press, Guelph, 1983.
2 G. C. Levy, *Topics in ^{13}C NMR Spectroscopy*, Wiley, New York, 1984, 1, ch. 3.
3 J. W. Gleeson and R. W. Vaughan, *J. Chem. Phys.*, 1983, **78**, 5384.
4 J. Mason, *Multinuclear NMR*, Plenum, New York, 1987, ch. 2.5.
5 P. S. Hubbard, *Phys. Rev.*, 1963, **131**, 1155.
6 S. Martinengo, D. Strumolo, P. Chini, V. Albano and D. Braga, *J. Chem. Soc., Dalton Trans.*, 1985, 35.
7 A. Abragam, *The Principles of Nuclear Magnetism*, Clarendon Press, Oxford, 1961.
8 B. T. Heaton, *Pure Appl. Chem.*, 1988, **60**, 1757 and refs. therein.
9 J. A. Creighton, R. Della Pergola, B. T. Heaton, S. Martinengo, L. Strona and D. Willis, *J. Chem. Soc., Chem. Commun.*, 1982, 864.
10 V. G. Albano, P. Chini, S. Martinengo, D. J. A. McCaffrey, D. Strumolo and B. T. Heaton, *J. Am. Chem. Soc.*, 1974, **96**, 8106.
11 B. T. Heaton, L. Strona and S. Martinengo, *J. Organomet. Chem.*, 1981, **215**, 415.
12 L. Merwin, Durham University, program based on procedure in M. M. Maricq and J. S. Waugh, *J. Chem. Phys.*, 1979, **70**(7), 3300.
13 L. H. Merwin, A. Sevald, J. E. Espidel and R. K. Harris, *J. Magn. Reson.* 1989, **84**, 367.
14 A. Cerriotti, G. Longoni, M. Manassero, M. Perego and M. Sansoni, *Inorg. Chem.*, 1985, **24**, 117.
15 V. G. Albano, P. Chini, S. Martinengo, M. Sansoni and D. Strumolo, *J. Chem. Soc., Chem. Commun.*, 1974, 299.
16 V. G. Albano, D. Braga and S. Martinengo, *J. Chem. Soc., Dalton Trans.*, 1986, 981.
17 V. G. Albano, M. Sansoni, P. Chini and S. Martinengo, *J. Chem. Soc., Dalton Trans.*, 1973, 651.
18 V. G. Albano, D. Braga and S. Martinengo, *J. Chem. Soc., Dalton Trans.*, 1981, 717.
19 R. E. Stevens, P. C. C. Like and W. L. Gladfelter, *J. Organomet. Chem.*, 1985, **287**, 133.
20 G. Ciani and S. Martinengo, *J. Organomet. Chem.*, 1986, **306**, C49.
21 R. Bonfichi, G. Ciani, A. Sironi and S. Martinengo, *J. Chem. Soc., Dalton Trans.*, 1983, 253.
22 J. C. Calabrese, L. F. Dahl, A. Cavalieri, P. Chini, G. Longoni and S. Martinengo, *J. Am. Chem. Soc.*, 1974, **96**, 2616.

Received 21*st November* 1994; *Paper* 4/07075E

* The isotropic shielding is related, through a sign change, to the chemical shift of the centreband of a spinning sideband pattern. Using equations (6) and (7), values for ζ and η are obtained such that $1 > \eta > 0$ holds; in the eventuality that η falls outside this range, the tensor elements σ_{zz}, σ_{xx} and σ_{yy} are reordered so that the convention $|\sigma_{zz} - \sigma_{iso}| > |\sigma_{xx} - \sigma_{iso}| > |\sigma_{yy} - \sigma_{iso}|$ applies. In this way σ_{zz} can be estimated unambiguously (providing that $\eta < 1$) as σ_{iso} lies between σ_{zz} and σ_{yy}. In the case of $\eta = 1$, $\sigma_{iso} = \sigma_{yy}$ and σ_{xx} and σ_{zz} are indistinguishable.